Octet-Line Node Structure of Superconducting Order Parameter in KFe_2As_2

K. Okazaki,[1,2]* Y. Ota,[1] Y. Kotani,[1,2] W. Malaeb,[1,3] Y. Ishida,[1] T. Shimojima,[4] T. Kiss,[5] S. Watanabe,[6] C.-T. Chen,[7] K. Kihou,[3,8] C. H. Lee,[3,8] A. Iyo,[3,8] H. Eisaki,[3,8] T. Saito,[9] H. Fukazawa,[3,9] Y. Kohori,[3,9] K. Hashimoto,[10]† T. Shibauchi,[10] Y. Matsuda,[10] H. Ikeda,[10] H. Miyahara,[4] R. Arita,[4] A. Chainani,[11,12] S. Shin[1,2,3,11]*

In iron-pnictide superconductivity, the interband interaction between the hole and electron Fermi surfaces (FSs) is believed to play an important role. However, KFe_2As_2 has three zone-centered hole FSs and no electron FS but still exhibits superconductivity. Our ultrahigh-resolution laser angle-resolved photoemission spectroscopy unveils that KFe_2As_2 is a nodal *s*-wave superconductor with highly unusual FS-selective multi-gap structure: a nodeless gap on the inner FS, an unconventional gap with "octet-line nodes" on the middle FS, and an almost-zero gap on the outer FS. This gap structure may arise from the frustration between competing pairing interactions on the hole FSs causing the eightfold sign reversal. Our results suggest that the A_{1g} superconducting symmetry is universal in iron-pnictides, in spite of the variety of gap functions.

KFe_2As_2 is the end member of the hole-doped $(Ba_{1-x}K_x)Fe_2As_2$ (BaK-122) series of pnictide superconductors. The optimally doped ($x \sim 0.4$) member of the series possesses the representative features of iron-based superconductors (*1*): an electronic structure that is derived from multiple Fe-3d orbitals and consists of hole Fermi-surface (FS) sheets around the zone center (Γ point), electron sheets around the zone corner (*X* point), and a fully gapped superconducting state (*2*, *3*). In KFe_2As_2 ($x = 1$, K122), for which there is experimental evidence (*4*–*6*) of gap nodes, the extreme hole doping changes the electron sheets to the clover-like hole pockets, which makes this material distinctly different from other iron-based systems, including the possible nodal superconductors LaFePO (*7*) and $BaFe_2(As,P)_2$ (*8*, *9*). This property of K122 has led to a recent theoretical suggestion of *d*-wave superconductivity with gap nodes in the all-zone–centered hole bands (*10*, *11*), which would imply a phase transition featuring a change in the superconducting gap symmetry from *s*- to *d*-wave as a function of doping *x*. In support of this picture, recent thermal conductivity measurements (*12*) suggest a possible

[1]Institute for Solid State Physics (ISSP), University of Tokyo, Kashiwa, Chiba 277-8581, Japan. [2]Core Research for Evolutional Science and Technology (CREST), Japan Science and Technology Agency (JST), Chiyoda-ku, Tokyo 102-0075, Japan. [3]Transformative Research-project on Iron Pnictides (TRIP), JST, Chiyoda-ku, Tokyo 102-0075, Japan. [4]Department of Applied Physics, University of Tokyo, Tokyo 113-8656, Japan. [5]Graduate School of Engineering Science, Osaka University, Osaka 560-8531, Japan. [6]Research Institute for Science and Technology, Tokyo University of Science, Chiba 278-8510, Japan. [7]Beijing Center for Crystal R&D, Chinese Academy of Science (CAS), Zhongguancun, Beijing 100190, China. [8]National Institute of Advanced Industrial Science and Technology (AIST), Tsukuba, Ibaraki 305-8568, Japan. [9]Department of Physics, Chiba University, Chiba 263-8522, Japan. [10]Department of Physics, Kyoto University, Sakyo-ku, Kyoto 606-8502, Japan. [11]RIKEN SPring-8 Center, Sayo-gun, Hyogo 679-5148, Japan. [12]Department of Physics, Tohoku University, Aramaki, Aoba-ku, Sendai 980-8578 Japan.

*To whom correspondence should be addressed. E-mail: okazaki@issp.u-tokyo.ac.jp (K.O.); shin@issp.u-tokyo.ac.jp (S.S.)

†Present address: Institute for Materials Research, Tohoku University, Sendai 980-8577, Japan.

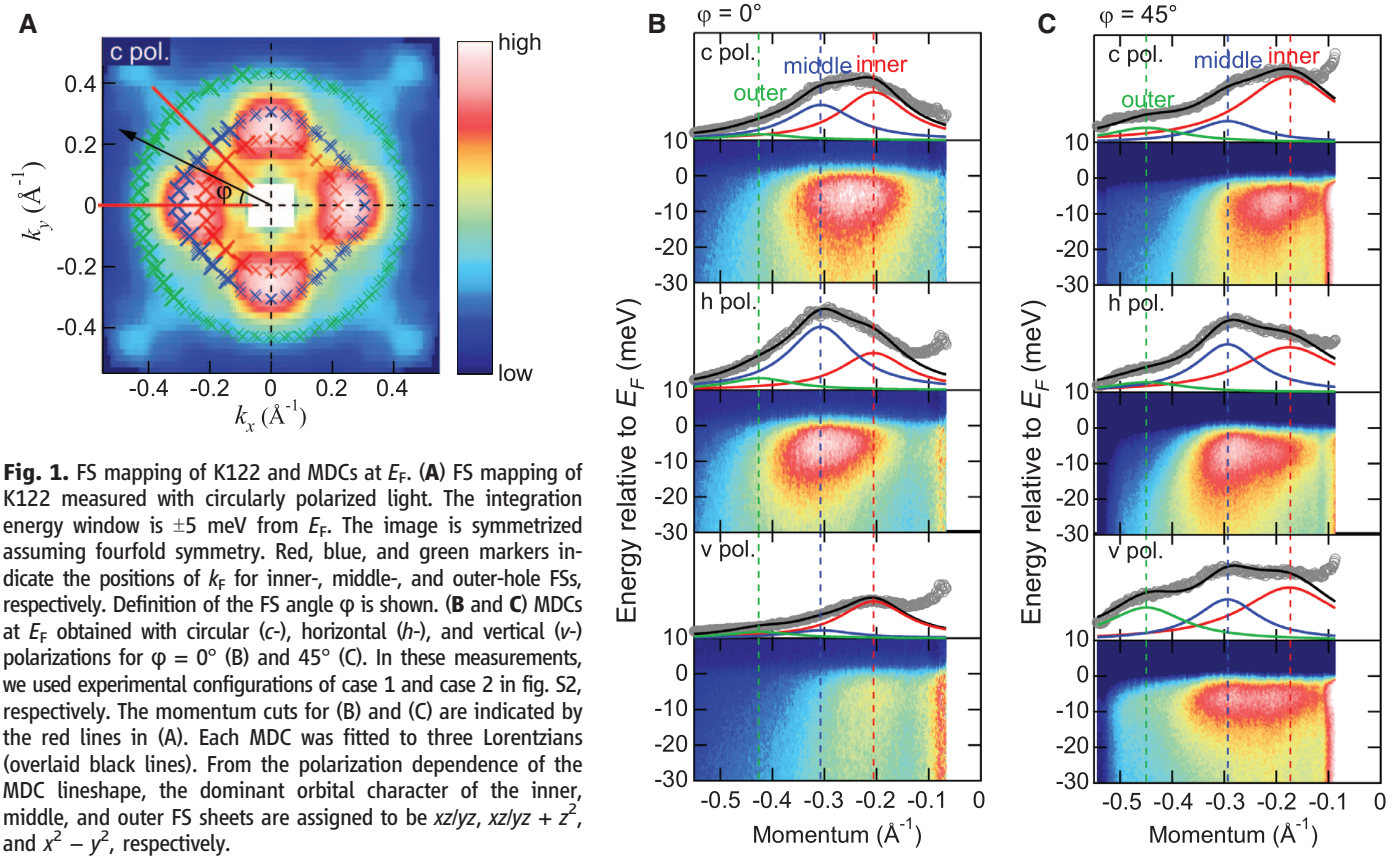

Fig. 1. FS mapping of K122 and MDCs at E_F. (**A**) FS mapping of K122 measured with circularly polarized light. The integration energy window is ±5 meV from E_F. The image is symmetrized assuming fourfold symmetry. Red, blue, and green markers indicate the positions of k_F for inner-, middle-, and outer-hole FSs, respectively. Definition of the FS angle φ is shown. (**B** and **C**) MDCs at E_F obtained with circular (*c*-), horizontal (*h*-), and vertical (*v*-) polarizations for φ = 0° (B) and 45° (C). In these measurements, we used experimental configurations of case 1 and case 2 in fig. S2, respectively. The momentum cuts for (B) and (C) are indicated by the red lines in (A). Each MDC was fitted to three Lorentzians (overlaid black lines). From the polarization dependence of the MDC lineshape, the dominant orbital character of the inner, middle, and outer FS sheets are assigned to be *xz*/*yz*, *xz*/*yz* + z^2, and $x^2 - y^2$, respectively.

d-wave gap symmetry in K122. It is therefore important to determine the gap symmetry and positions of the nodes in the Brillouin zone of K122.

Recently, we have developed a laser-excited angle-resolved photoemission spectroscopy (laser ARPES) apparatus that achieves a maximum energy resolution of 70 μeV and lowest cooling temperature of 1.5 K (*13*). This high-energy resolution indicates very high stability of the Fermi level (E_F) position, enabling a direct measurement of the superconducting (SC) gap of K122, which has a critical temperature (T_c) as low as 3.4 K (*14*).

We first resolve and analyze the FSs of K122 around the Brillouin-zone (BZ) center. The FS map of K122 is shown in Fig. 1A, with an energy resolution of 4 meV with circularly polarized light, and the momentum distribution curves (MDCs) at E_F are shown in Fig. 1, B and C, measured with the circularly (*c*), horizontally (*h*), and vertically (*v*) polarized light (definition of polarization is provided in fig. S2) for the cuts along the azimuth angles 0° and 45°, respectively (Fig. 1A). Each MDC can be fitted to three Lorentzians, resolving three-hole FSs around the BZ center as predicted with band-structure calculations (*15*, *16*). The Fermi momentum (k_F) obtained (symbols) from the fits are overlaid on the FS map in Fig. 1A (the determination of the k_F positions of the other cuts are provided in fig. S3). The MDC line shapes depend on the polarization of the incident laser because of the parity selection rules, and accordingly, we can determine the dominant orbital character of the inner-, middle-, and outer-FS sheets to be *xz*/*yz*, *xz*/*yz* + z^2, and $x^2 - y^2$, respectively (*13*).

The energy distribution curves (EDCs) at k_F of the inner, middle, and outer FSs measured at 2.0 K (below T_c) are shown in Fig. 2, A to C. Each EDC at k_F is identified with a FS angle ϕ (Fig. 1A). The k_F positions were obtained from MDCs measured with a lower resolution of 4 meV and confirmed by the quasiparticle behavior seen in the EDCs measured at 2.0 K, below T_c (EDCs of representative cuts are provided in fig. S6). The EDCs shown in Fig. 2, A to C, were symmetrized with respect to E_F, and the results are shown in Fig. 2, D to F, respectively. The valley structures at E_F observed in the symmetrized EDCs of the inner FS (Fig. 2D) indicate the opening of a SC gap for all FS angles with some anisotropy in the gap size. For the middle FS, the symmetrized EDCs in Fig. 2E show peaks or valleys at E_F as a function of FS angle, indicating that the SC gap is more anisotropic and is almost closed around φ = 0° (*17*). For the outer FS, the symmetrized EDCs show a peak structure for all angles in Fig. 2F, indicating that the size of the SC gap seems to be almost zero for all FS angles. Thus, there is a clear FS sheet dependence in the SC-gap size of K122, which is in strong contrast to the optimally doped BaK-122 (*18*) but is consistent with the evolution of the gaps as a function of K doping (*19*). In order to quantify the SC-gap size, we have fitted the EDCs to the Dynes' function (*20*). Although this function is appropriate for the density of states, we have also confirmed that all the EDCs can be fitted to the Bardeen-Cooper-Schrieffer (BCS) spectral function used in (*18*), and they give almost the same SC-gap sizes [a comparison of the Dynes' and spectral function fits and the reason why we chose the Dynes function is given in (*13*)]. We were able to fit all of the EDCs to calculated spectra (Fig. 2, solid lines) (*21*).

To confirm whether or not the gap is really closed around φ = 0° of the middle FS, we performed detailed measurements in this region with increased accuracy of the E_F position. We show the EDCs and symmetrized EDCs in Fig. 3, A and B, respectively, for φ = 8.9°, 4.0°, and –0.5°; the solid lines indicate the fits to the Dynes' function. The spectra at φ = 8.9° and –0.5° acquire small but finite SC gaps, whereas the gap is closed around φ = 4.0°. Furthermore, we have measured the temperature dependence of the spectra. The EDCs above and below T_c close to the node (φ = 5.0°) and off the node (φ = 22.7°) are shown in Fig. 3, C and D, respectively. The leading edge does not shift for the EDCs near the node, but a finite shift can be observed for the EDCs off the node. This indicates that the nodal points exist around φ = 5.0°.

We plot the SC-gap sizes derived from the Dynes' function fits as a function of FS angle in Fig. 4A. The solid circles are derived from the EDCs shown in Fig. 2, and the open circles are plotted by symmetrizing the data, taking into

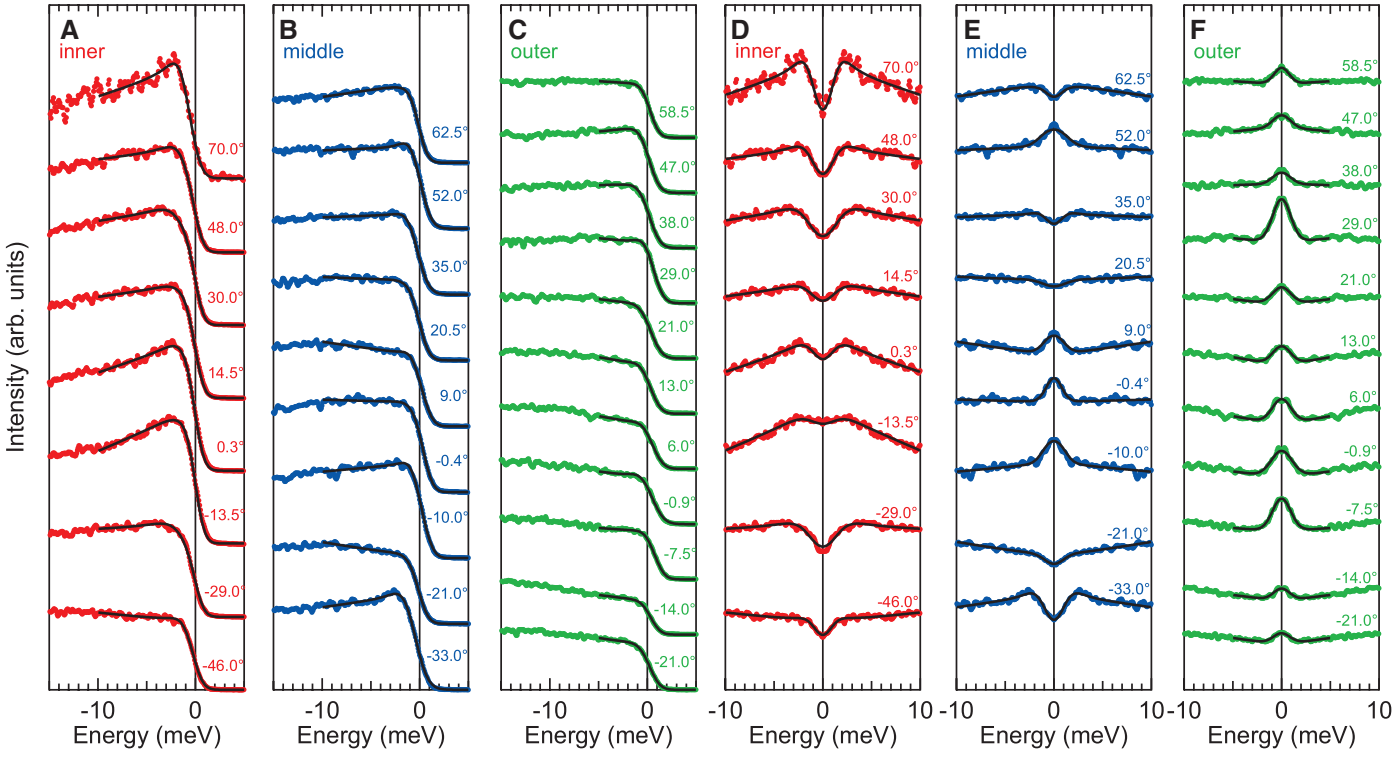

Fig. 2. EDCs and symmetrized EDCs at k_F. (**A** to **C**) EDCs at k_F of (A) inner, (B) middle, and (C) outer FSs, respectively, taken at 2.0 K (<T_c = 3.4 K) for various FS angles as shown in each panel. The integration angle window is ± 0.5° (~ ± 0.0075 Å^{-1}) from k_F. (**D** to **F**) Symmetrized EDCs of (D) inner, (E) middle, and (F) outer FSs, respectively. By symmetrization, the temperature dependence of the FD function can be canceled out so that the symmetrized EDCs approximately reflect the spectral functions around E_F. The fits to the Dynes' function are indicated by the solid lines.

account the tetragonal crystal symmetry. In addition, the results of several high-resolution measurements around φ ~ 0° for the inner and middle FSs are also plotted with open rectangles, triangles, and diamonds. In the inset, the SC gaps around φ ~ 0° of the middle FS are plotted on an enlarged scale. First of all, a fully gapped structure without nodes on the inner FS is consistent with the *s*-wave symmetry and excludes the *d*-wave symmetry with nodes as suggested theoretically (*10*, *11*) and experimentally (*12*). In addition, the SC gap structure on the inner and middle FSs shows strong anisotropy, whereas that on the outer FS is vanishingly small. To obtain insight into the angle dependence of these SC gap functions, we have tried to fit them with two lowest harmonics under the fourfold tetragonal symmetry

$$\Delta(\varphi) = |\Delta_0[1 + A\cos(4\varphi) + B\cos(8\varphi)]| \quad (1)$$

Such cos(4φ) term has been considered in some theoretical works (*22*, *23*). In our case, the inclusion of the higher-order cos(8φ) term is required to reproduce the gap minima observed around 0° and 45°. As shown in Fig. 4A, we find that this simple analysis successfully explains the experimental data (*24*). The obtained gap functions are depicted in Fig. 4B. The nodal points in the middle FS are located at φ = ±(5.34 ± 0.04)° (fitting parameters are in Table 1). We have confirmed that these gap functions are consistent with the London penetration depth results (fig. S9). Thus, we conclude that K122 is a nodal *s*-wave multi-gap superconductor with unusual eightfold sign reversal in a gap function. This implies that in spite of the large variety of gap functions even within the 122 family, the basic symmetry of the superconducting order parameter always belongs to the A_{1g} representation, which is symmetrical with respect to fourfold rotation (*25*).

On the basis of the above results of the SC-gap structure in K122, it was important to ensure that surface effects can be excluded in our observations. It is widely accepted that laser ARPES using very low-energy photons ($h\nu$ = 6.998 eV, as in the present case) is bulk-sensitive, which is in contrast to conventional ARPES measurements that use higher-energy photons. We have further checked that the FS size of the present compound K122 determined with our laser ARPES is nearly same as those determined with de Haas-van Alphen oscillations, which measures bulk properties (*15*). Moreover, the determined SC-gap structure well reproduces the previously reported London penetration depth results (fig. S9). In addition, we have performed systematic measurements of the FSs, MDCs, and EDCs at T = 10 K (figs. S10 and S11), which indicate very good consistency with the data measured below T_c = 3.4 K. These results confirm that our measurements do indeed probe the bulk electronic structure and FSs, thus ensuring that surface effects can be safely excluded in our observations.

Given the importance of intra- and interorbital interactions and proximity of the FSs in momentum space (*10*, *11*, *26*, *27*), the almost-zero gap on the outer FS and the largest gap on the inner FS compared with the middle FS may seem inconsistent at first glance. However, we believe that this is quite consistent with the multi-orbital character of the FSs of iron-based superconductors: The inner and middle FSs have a predominantly *xz*/*yz* and *xz*/*yz* + z^2 character, respectively. The existence of strong FS-sheet dependence in the SC-gap size and the presence of SC-gap nodes may indicate that there is some frustration between competing pairing interactions on the hole FSs. This can be consistently explained by considering inter- and intra-band repulsive interactions mediated by spin fluctuations (*11*, *26*, *27*) as follows. Although we have not measured the FS near the zone corner, it has been suggested both experimentally and theoretically that the interband scattering between the zone-center bands and the zone-corner bands can still be important (*28*). In (*28*), incommensurate spin fluctuations have been observed by means of inelastic neutron scattering with a wave vector approximately corresponding to that from the BZ center (Γ point) to the BZ corner (*X* point). The middle FS has finite contributions from the z^2 orbital, whereas the clover-like FSs at *X* point have almost no contribution from this orbital (Fig. 4B and fig. S5). Hence, the z^2-orbital component in the middle FS has no counterpart for the sign change of SC gap in the clover-like FSs. As a result, an intra-FS sign change may be preferable for the SC gap of the middle FS around the momentum region with a large z^2 orbital contribution. This scenario can also explain the SC-gap size of the inner and outer FSs. From the density functional theory calculations, the dominant contributions to the clover-like FSs are *xz*/*yz* orbitals. Because the inner FS also has dominantly *xz*/*yz* character, the inter-FS pairing interactions should be the strongest leading to the largest gap size for the inner FS. For the outer FS having large $x^2 - y^2$ orbital contribution, the corresponding contribution is almost absent in the partner clover-like FSs, which is consistent with the negligibly small gap size on the outer FS, as observed in this study. In addition, this band has a relatively large renormalization effect (*15*), which may reduce the gap size.

In a recent study investigating the relation between spin fluctuations and superconductivity,

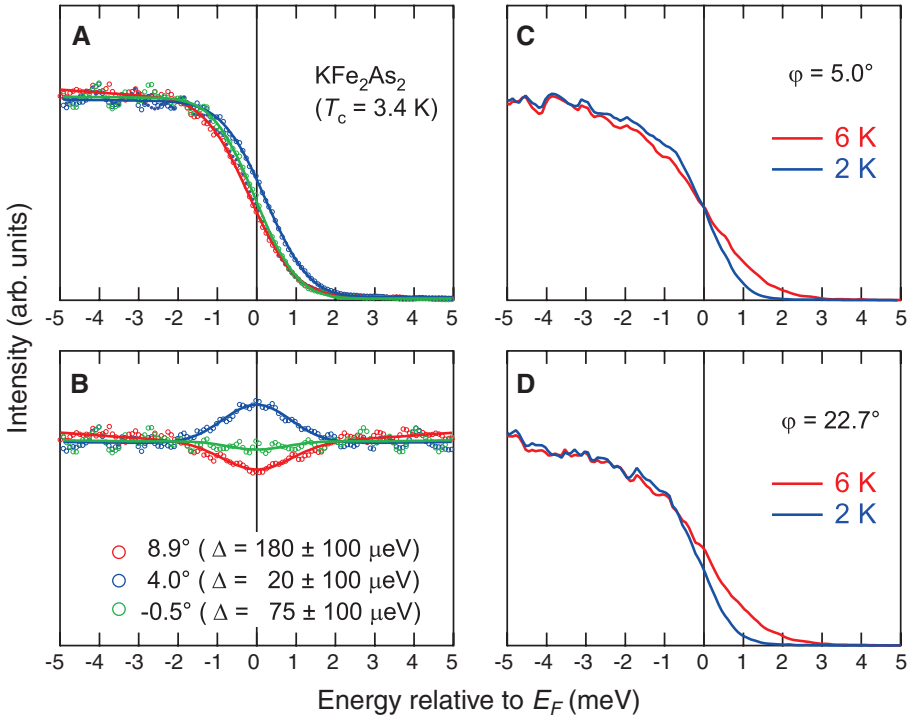

Fig. 3. (**A**) EDCs and (**B**) symmetrized EDCs at k_F of the middle FS for φ = 8.9°, 4.0°, and −0.5° are indicated by red, blue, and green symbols, respectively. The fits to the Dynes' function are indicated by the solid lines in (A and B), and the estimated SC-gap sizes are listed in (B). (**C** and **D**) Temperature-dependent EDCs above and below T_c (C) near the nodal point (φ = 5.0°) and (D) for an off-nodal point (φ = 22.7°).

Table 1. Fitting parameters for Fig. 4A. k_B is the Boltzmann constant.

	Δ_0 (meV)	$2\Delta_0/k_BT_c$	A	B
Inner FS	1.11 ± 0.05	7.58 ± 0.34	−0.12 ± 0.06	−0.17 ± 0.05
Middle FS	0.41 ± 0.05	2.80 ± 0.34	−0.40 ± 0.14	−0.85 ± 0.18
Outer FS	0.15 ± 0.06	1.02 ± 0.41	−0.01 ± 0.57	−0.26 ± 0.58

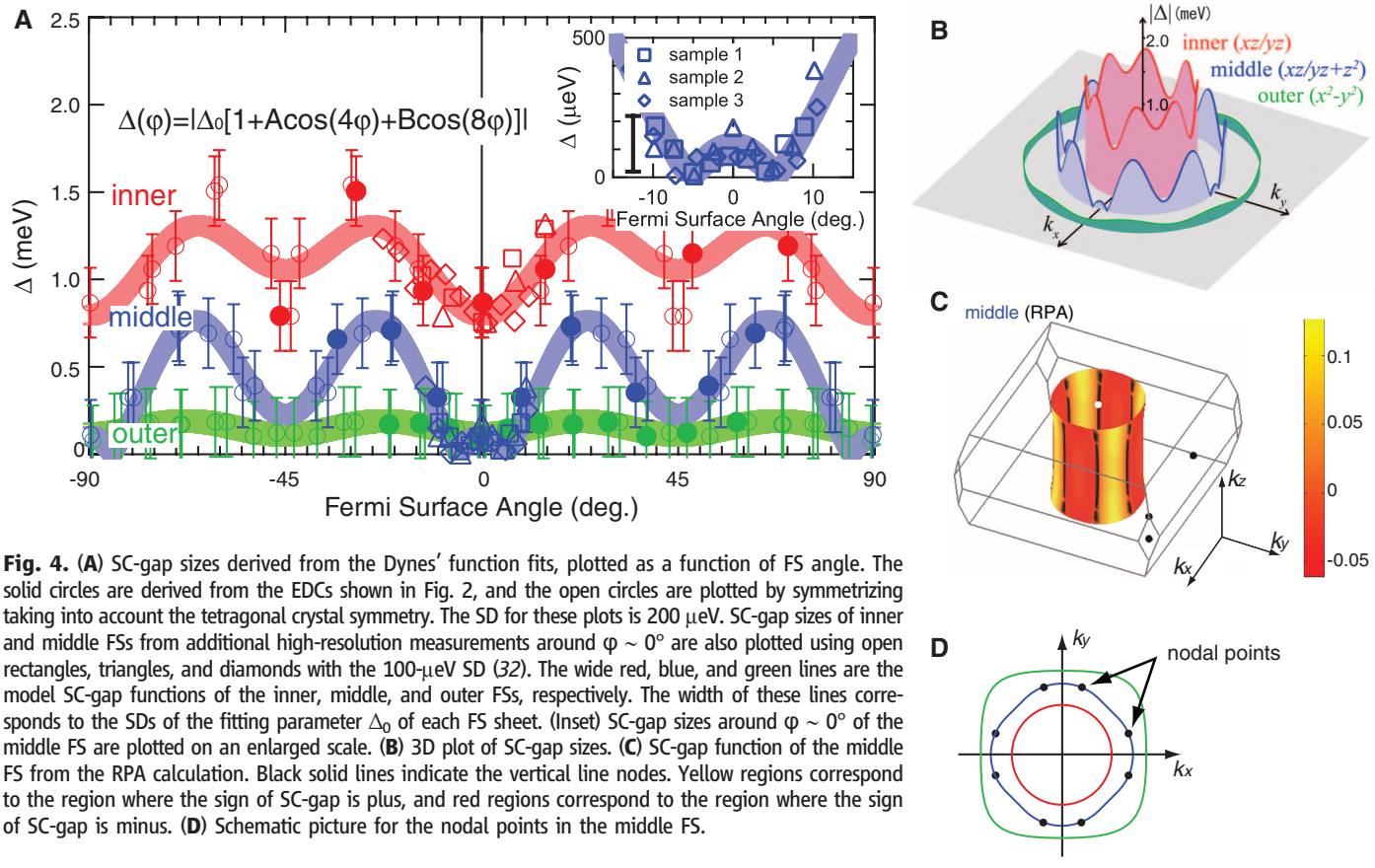

Fig. 4. (**A**) SC-gap sizes derived from the Dynes' function fits, plotted as a function of FS angle. The solid circles are derived from the EDCs shown in Fig. 2, and the open circles are plotted by symmetrizing taking into account the tetragonal crystal symmetry. The SD for these plots is 200 μeV. SC-gap sizes of inner and middle FSs from additional high-resolution measurements around φ ~ 0° are also plotted using open rectangles, triangles, and diamonds with the 100-μeV SD (*32*). The wide red, blue, and green lines are the model SC-gap functions of the inner, middle, and outer FSs, respectively. The width of these lines corresponds to the SDs of the fitting parameter Δ_0 of each FS sheet. (Inset) SC-gap sizes around φ ~ 0° of the middle FS are plotted on an enlarged scale. (**B**) 3D plot of SC-gap sizes. (**C**) SC-gap function of the middle FS from the RPA calculation. Black solid lines indicate the vertical line nodes. Yellow regions correspond to the region where the sign of SC-gap is plus, and red regions correspond to the region where the sign of SC-gap is minus. (**D**) Schematic picture for the nodal points in the middle FS.

random phase approximation (RPA) was used to obtain the spin susceptibility and solve the linearized Eliashberg equation (*29*), showing that the FS with substantial z^2 contribution has a horizontal node around $k_z = \pi$. However, recently, it has been shown that horizontal nodes can appear on the middle FS by a phenomenological calculation (*25*). By RPA calculation, we also found that the horizontal node on the middle FS around $k_z = \pi$ becomes loop nodes and eventually vertical nodes if we introduce an orbital-dependent potential that mimics the self-energy effect (Fig. 4C and fig. S6). From a comparison with the three-dimensional (3D) ARPES study of Yoshida *et al.* (*16*), we conclude that the k_z value for our 7-eV photon is very close to π (*30*). If the nodal lines make a loop around $k_z = \pi$, the SC-gap nodes should be smeared out because of the k_z broadening effect (*31*). Therefore, the nodal lines are likely running almost vertically around the FS angle φ ~ ±5° (Fig. 4D).

References and Notes

1. Y. Kamihara, T. Watanabe, M. Hirano, H. Hosono, *J. Am. Chem. Soc.* **130**, 3296 (2008).
2. H. Ding *et al.*, *Europhys. Lett.* **83**, 47001 (2008).
3. K. Nakayama *et al.*, *Europhys. Lett.* **85**, 67002 (2009).
4. H. Fukazawa *et al.*, *J. Phys. Soc. Jpn.* **78**, 083712 (2009).
5. J. K. Dong *et al.*, *Phys. Rev. Lett.* **104**, 087005 (2010).
6. K. Hashimoto *et al.*, *Phys. Rev. B* **82**, 014526 (2010).
7. J. D. Fletcher *et al.*, *Phys. Rev. Lett.* **102**, 147001 (2009).
8. K. Hashimoto *et al.*, *Phys. Rev. B* **81**, 220501 (2010).
9. Y. Zhang *et al.*, *Nat. Phys.* **8**, 371 (2012).
10. R. Thomale, C. Platt, W. Hanke, J. Hu, B. A. Bernevig, *Phys. Rev. Lett.* **107**, 117001 (2011).
11. S. Maiti, M. M. Korshunov, T. A. Maier, P. J. Hirschfeld, A. V. Chubukov, *Phys. Rev. Lett.* **107**, 147002 (2011).
12. J.-Ph. Reid *et al.*, http://arxiv.org/abs/1201.3376v1 (2012).
13. Materials and methods are available as supplementary materials on *Science* Online.
14. K. Kihou *et al.*, *J. Phys. Soc. Jpn.* **79**, 124713 (2010).
15. T. Terashima *et al.*, *J. Phys. Soc. Jpn.* **79**, 053702 (2010).
16. T. Yoshida *et al.*, *J. Phys. Chem. Solids* **72**, 465 (2011).
17. The symmetrized EDC of the middle FS show a peak also at φ = 52°. However, for this FS angle the fitting gave a small but finite SC-gap size.
18. T. Shimojima *et al.*, *Science* **332**, 564 (2011).
19. W. Malaeb *et al.*, http://arxiv.org/abs/1204.0326v1 (2012).
20. R. C. Dynes, V. Narayanamurti, J. P. Garno, *Phys. Rev. Lett.* **41**, 1509 (1978).
21. When the SC-gap size is much smaller than the broadening width of the Fermi-Dirac (FD) function, the symmetrized EDC can be a peak-like line shape at E_F.
22. S. Graser, T. A. Maier, P. J. Hirschfeld, D. J. Scalapino, *N. J. Phys.* **11**, 025016 (2009).
23. S. Maiti, A. V. Chubukov, *Phys. Rev. B* **82**, 214515 (2010).
24. We have confirmed that even if we try fitting including a higher-order modulation such as cos(16φ), the position of the nodal points is almost unaffected.
25. S. Maiti, M. M. Korshunov, A. V. Chubukov, *Phys. Rev. B* **85**, 014511 (2012).
26. I. I. Mazin, D. J. Singh, M. D. Johannes, M. H. Du, *Phys. Rev. Lett.* **101**, 057003 (2008).
27. K. Kuroki *et al.*, *Phys. Rev. Lett.* **101**, 087004 (2008).
28. C. H. Lee *et al.*, *Phys. Rev. Lett.* **106**, 067003 (2011).
29. K. Suzuki, H. Usui, K. Kuroki, *Phys. Rev. B* **84**, 144514 (2011).
30. The shape of the middle FS from our ARPES study using 7-eV photons is similar to that around the *Z* point measured with 3D-ARPES. Furthermore, according to 3D-ARPES the middle FS shows warping just near the *Z* point only around the region of FS angle ~ 45°. If our ARPES results using 7-eV photons had traced the warping region, the MDC width of the middle FS at E_F should be broader for azimuth angle = 45°. However, the MDC width of the middle FS at E_F is not so different between that for azimuth angle = 0° and for azimuth angle = 45°, thus confirming that our ARPES results using 7-eV photons shoud trace the ragion very close to the *Z* point.
31. Because the escape depth of the photoelectrons is finite, k_z value of photoelectrons is not conserved but is broadened. k_z value of the observed photoelectrons should be integrated within 10 to 20% of the whole BZ region, considering that the escape depth of photoelectrons for 7-eV laser is ~30 to 70 Å, whereas the unit cell length along the *c* axis is ~14 Å.
32. We have confirmed that SD of the SC-gap value obtained through least-square fitting is below 1 μeV by assuming that the detected counts of photoelectrons obey Poisson distribution.

Acknowledgments: We thank K. Kuroki, T. Yoshida, and S. Kittaka for valuable discussions; A. V. Chubukov for valuable comments; and T. Kondo for reading the manuscript and comments. This research is supported by the Japan Society for the Promotion of Science (JSPS) through its FIRST Program. C.H.L. was additionally supported by Grant-in-Aid for Scientific Research B (No. 24340090) from JSPS. H.F. was additionally supported by Grants-in-Aid for Scientic Research (21540351 and 22684016) from the Ministry of Education, Culture, Sports, Science and Technology (MEXT) and JSPS and Innovative Areas "Heavy Electrons" (20102005 and 21102505) from MEXT. T.S. was additionally supported by Grant-in-Aid for the Global COE program "The Next Generation of Physics, Spun from Universality and Emergence" from MEXT, and KAKENHI from JSPS.

Supplementary Materials

www.sciencemag.org/cgi/content/full/337/6100/1314/DC1
Materials and Methods
Figs. S1 to S11
Tables S1 and S2
References (*33*–*43*)

3 April 2012; accepted 25 July 2012
10.1126/science.1222793

Science

Octet-Line Node Structure of Superconducting Order Parameter in KFe_2As_2

K. Okazaki, Y. Ota, Y. Kotani, W. Malaeb, Y. Ishida, T. Shimojima, T. Kiss, S. Watanabe, C.-T. Chen, K. Kihou, C. H. Lee, A. Iyo, H. Eisaki, T. Saito, H. Fukazawa, Y. Kohori, K. Hashimoto, T. Shibauchi, Y. Matsuda, H. Ikeda, H. Miyahara, R. Arita, A. Chainani and S. Shin

Science **337** (6100), 1314-1317.
DOI: 10.1126/science.1222793

An Eight-Noded Monster

In superconductors, electrons are bound into pairs, and the exact form of that pairing and the resulting energy gap can vary, depending on the details of the electron-electron interaction and the band structure of the material. The energy gaps of the recently discovered iron-based superconductors exhibit a variety of pairing functions. KFe_2As_2 has been suggested to have a *d*-wave gap, similar to cuprate superconductors. **Okazaki *et al.*** (p. 1314) use laser-based angle-resolved photoemission spectroscopy (ARPES) to map out the superconducting gap on three Fermi surfaces (FS) of the compound. They find a different gap structure on each, with the middle FS gap vanishing at eight distinct positions (nodes). It appears that the gap respects the tetragonal symmetry of the crystal, indicating (although the details may vary) the all iron-based superconductors have an extended *s*-wave–symmetric pairing—a finding that will help understanding of unconventional superconductivity.